JOURNAL OF MATERIALS SCIENCE 33 (1998) 1333–1341

Ageing characteristics of Cu–Cr *in-situ* composite

Y. JIN, K. ADACHI, T. TAKEUCHI, H. G. SUZUKI
Mechanical Properties Division, National Research Institute for Metals, Tsukuba, Ibaraki 305, Japan
E-mail: yjin@andrew.cmu.edu

The ageing behaviour of a Cu–15 wt% Cr *in-situ* composite was investigated systematically by means of hardness testing, electrical conductivity measurement, scanning electron microscopy, analytical transmission electron microscopy and high-resolution electron microscopy. The material was found to have a peak hardness after ageing at around 773 K and a peak electrical conductivity at around 873 K. In contrast with the dilute Cu–Cr alloys, Cr-rich clusters were observed at the early aged condition in the Cu matrix, which matches not only the results of mechanical and physical property measurement but also the theoretical prediction. In addition, the precipitates at peak hardened condition in the Cu matrix were determined to be Cr Guinier–Preston zones. Cr ribbon as the *in-situ* reinforcing element shows no measurable ageing effect due to the high-temperature solution treatment.

1. Introduction

High-strength (greater than 1 GPa) and highly conductive (greater than 80% of the International Annealed Copper Standard (IACS)) material has a strong application potential in the automobile, electrical and electronic industries. In order to reach this goal, extensive studies are now being carried out on various Cu–Nb [1–10], Cu–Fe [11–16], Cu–Ag [17–20] and Cu–Cr [21–25] *in-situ* composites which have much higher concentrations of the secondary element than the dilute Cu alloys. In these materials, heavy cold working and ageing are two most important materials-processing techniques. By heavy cold working, the as-cast dendrites can be deformed into reinforcing elements (fibres or ribbons) for obtaining high strength. By the ageing treatment, the conductivity of the material can be greatly improved. However, to the present authors' knowledge, there are still no reports concerning the ageing characteristics of Cu–Cr *in-situ* composite, although numerous results [26–39] have been published on dilute Cu–Cr alloys. Thus, it was necessary to clarify the difference between ageing behaviours of the two types of material.

Concerning the Cr precipitation in dilute Cu–Cr alloys, two problems remain unsolved.

(a) Although significant ageing effects are observed from 673 to 773 K, microstructurally no precipitates are seen until 748 K [26–29]. On the other hand, Kamijo and co-workers [30–33] predicted by the theoretical calculation of free energy that homogeneous nucleation should happen owing to the compositional fluctuation. The critical size and Cr concentration of the nuclei were calculated to be about 1 nm and 70.2 at% at 673 K in Cu–0.6 at% Cr alloy (the modified Borelius model).

(b) Different arguments exist concerning the crystal structure of metastable precipitates up to the peak hardness. As sufficient evidence has not yet been obtained, some researchers [28, 30–33] believe that the metastable precipitates have the same face-centred cubic (f.c.c.) lattice structure as that of the Cu matrix, while others [29, 34–36] suggest the same body-centred cubic (b.c.c.) lattice structure as that of pure Cr. In the overaged condition, it is generally agreed that the rod-like precipitate phase has the same b.c.c. structure as that of pure Cr and possesses a Kurdjumov–Sachs (KS) orientation relationship with the Cu matrix.

In the present work, we have investigated the above problems by means of hardness testing, electrical conductivity measurement, scanning electron microscopy (SEM), analytical transmission electron microscopy (TEM) and high-resolution electron microscopy (HREM).

2. Experimental procedure

The material was prepared by melting the high-purity (99.99 at%) Cu and high-purity (99.99 at%) Cr in a vacuum furnace at 1813 K to a nominal composition of Cu–15 wt% Cr. The ingot was hot forged at 1173 K and cold rolled into wires and sheets with a total reduction of up to 99.9%. The samples were solution treated under vacuum at 1273 K for 1 h, quenched into water and then aged under vacuum at different temperatures ranging from 473 to 1173 K, and different times ranging from 0.5 to 10 h.

The hardness test was performed on an MVK-H2 tester while the electrical conductivity was measured with the conventional four-point method at a constant current of 100 mA. The SEM samples were prepared by standard mechanical polishing methods and were etched in a solution of 15 vol% HCl, 5 vol% H_2SO_4 and 10 vol% HNO_3 with the balance water. The TEM samples were prepared by conventional electropolishing

method using an electrolyte of 20 vol% HNO_3 and 80 vol% CH_3OH at $-40\,^{\circ}C$. The SEM observation was conducted in a JSM-5400 scanning electron microscope with an accelerating voltage of 30 kV. The analytical TEM and HREM observations were carried out in a JEM-2000FXII transmission electron microscope and a JEM-2000EXII transmission electron microscope, respectively, with an accelerating voltage of 200 kV.

3. Results and discussion

3.1. Hardness testing

Fig. 1 shows the effect of ageing temperature on the hardness of the *in-situ* composite. It can be seen that the hardness stays constant until around 500 K, reaches a peak hardness at around 773 K and decreases rapidly at the higher ageing temperatures. The effect of ageing time on the hardness of the material has also been examined, with the results displayed in the inset. At an ageing temperature of 773 K, the hardness increases rapidly in the first hour and then gradually approaches a constant level. This trend is quite similar to that of dilute Cu–Cr alloys [26]. In addition, the corresponding microhardness testing on the Cu matrix and the Cr ribbon indicates that the Cu matrix has a similar ageing behaviour while the Cr ribbon displays no measurable ageing effect.

3.2. Electrical conductivity measurement

Fig. 2 shows the effect of ageing temperature on the electrical conductivity of the *in-situ* composite. It can be seen that the electrical conductivity starts to increase significantly at around 673 K, reaches a maximum at around 873 K and then decreases significantly at the higher ageing temperatures. The effect of ageing time on the electrical conductivity of the *in-situ* composite has also been examined. As displayed in the inset, at an ageing temperature of 773 K, the electrical conductivity increases rapidly in the first hour and then gradually becomes stable. This trend is also very similar to that of dilute Cu–Cr alloys [26].

3.3. Scanning electron microscopy observation

Fig. 3 shows the back-scattering electron images of the *in-situ* composite in the longitudinal cross-section (LC), aged for 1 h at different temperatures ranging from 293 to 1173 K. The rolling direction (RD) is also indicated. The Cr phase is darker than the Cu matrix since the atomic number of Cr is smaller than that of Cu. It can be seen that the material is composed of the Cr ribbons A with a thickness of around 0.1 μm, the spheroidized Cr phase B with a size of around 0.1 μm, the remains of highly deformed Cr dendrites C with a size of around 1 μm, and the Cu matrix (bright phase). However, no significant differences were observed in these specimens. The samples have also been examined in the transverse cross-section. A similar conclusion was obtained.

3.4. Analytical transmission electron microscopy observation

3.4.1. Cu matrix

The bright-field (BF) image of the Cu matrix in the *in-situ* composite aged at 473 K for 1 h is shown in Fig. 4a. No precipitates but the dislocations A introduced by water quenching can be seen. This is consistent with the results of hardness testing and electrical conductivity measurement since no significant ageing effect was detected yet. Fig. 4b is the BF image of the Cu matrix aged at 673 K for 1 h. In contrast with the

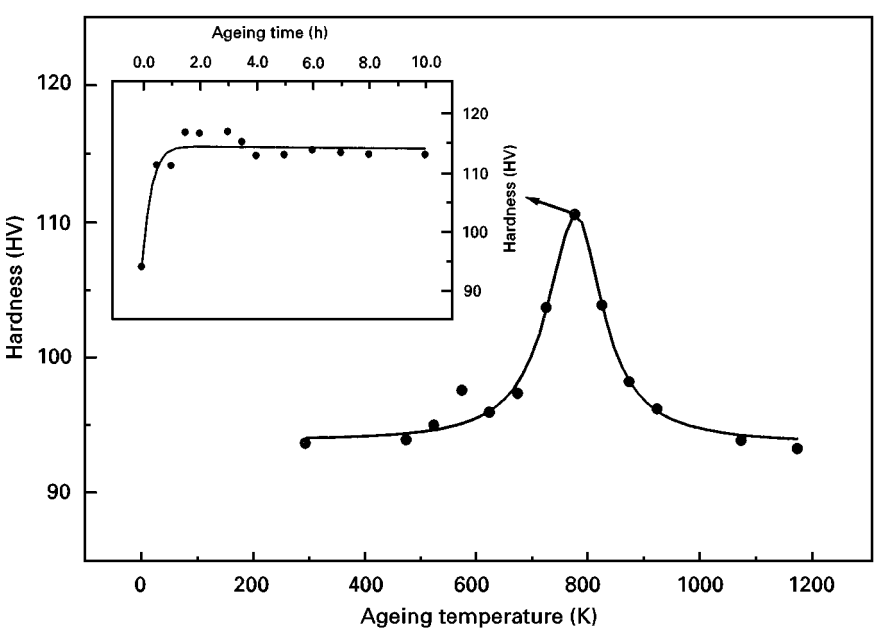

Figure 1 Effect of the ageing temperature (for 1 h) on the Vickers hardness of the *in-situ* composite. The inset shows the effect of the ageing time (at 773 K) on the hardness.

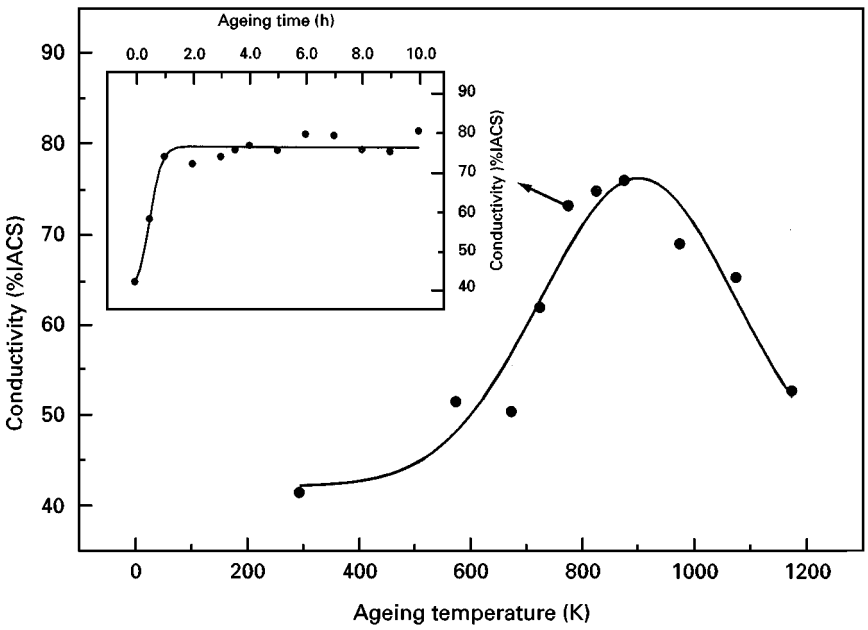

Figure 2 Effect of the ageing temperature (for 1 h) on the electrical conductivity of the *in-situ* composite. The inset shows the effect of the ageing time (at 773 K) on the electrical conductivity.

previous work on dilute Cu–Cr alloys [26–28], nanoscale Cr-rich clusters B were observed although their size is too small to produce a significant coherent spherical strain contrast (coffee-bean contrast) [40]. Since the corresponding hardness testing and electrical conductivity measurement have displayed a significant ageing effect, some evidence of precipitation should be seen microstructurally. The existence of these Cr-rich clusters also confirms the prediction of Kamijo and co-workers [30–33] on the basis of the free-energy theory. Although the existence of clusters at the initial stage of precipitation has been reported in many other materials [41–44], to the present authors' knowledge, this is the first experimental evidence in the binary Cu–Cr alloy system.

Fig. 4c shows the BF image of the Cu matrix in the peak hardened condition (773 K for 1 h). In contrast with the material in the underaged condition, typical coffee-bean contrast C was observed, suggesting that these precipitates are fully coherent with the Cu matrix and possess the same f.c.c. lattice and thus are designated as the Cr Guinier–Preston (GP) zones. Fig. 4d is the BF image of the Cu matrix at the peak electrical conductivity condition (873 K for 1 h). Unlike the case for the peak hardened condition, most of the precipitates D were found to be needle like with an associated high strain field. The observed phenomenon is similar to that of dilute Cu–Cr alloys at the same ageing temperature. It has been well proved by Weatherly *et al.* [29] that these precipitates are the Cr phase of b.c.c. crystal structure coherent with the Cu matrix along the longitudinal direction. Fig. 4e is the BF image of the Cu matrix held at 973 K for 1 h. Unlike the peak electrical conductivity condition, incoherent rod-shaped precipitates E were observed. The observed precipitates are also similar to that of dilute Cu–Cr alloys at the same ageing temperature. They have been determined as the incoherent Cr phase of b.c.c. crystal structure with a KS orientation relationship [26–28, 34–39]. Fig. 4f shows the BF image of the Cu matrix at an even higher ageing temperature (1073 K for 1 h). Only a small number of large incoherent Cr b.c.c. precipitates F can be observed. Since all the BF images displayed in Fig. 4 are close to $\langle 0\,1\,1\rangle_{Cu}$ orientation, the average size and spacing of these Cr precipitates were measured, and the results are summarized in Table I. Because there is a high strain field around the Cr-rich clusters and Cr GP zones, their values measured by means of TEM would be considerably larger than the actual size of these precipitates. This problem has been clarified by further studying them on an atomic scale with HREM techniques. The results are presented in Section 3.5.

As mentioned in Section 1, there is still some disagreement concerning the crystal structure of the Cr precipitates in the peak hardened condition. Some researchers [28, 30–33] believe that the metastable precipitates have the same f.c.c. lattice structure as that of the Cu matrix, while others [29, 34–36] suggest the same b.c.c. lattice structure as that of pure Cr. In order to clarify this point, a selected-area diffraction (SAD) analysis was carried out. Since the diffraction effect of precipitates strongly depends on the orientation of matrix, the SAD patterns from the same area of the Cu matrix in the peak hardened condition (773 K for 1 h) were examined systematically by tilting the specimen along its main reciprocal axes to cover all the possibilities. Fig. 5 shows the observed SAD patterns for the three major zones of [0 0 1], [0 1 1] and [1 1 1]. Although the SAD patterns have been exposed at different times, neither the diffuse diffraction streaks nor the diffraction spots other than those of the Cu matrix can be seen. This agrees well with the

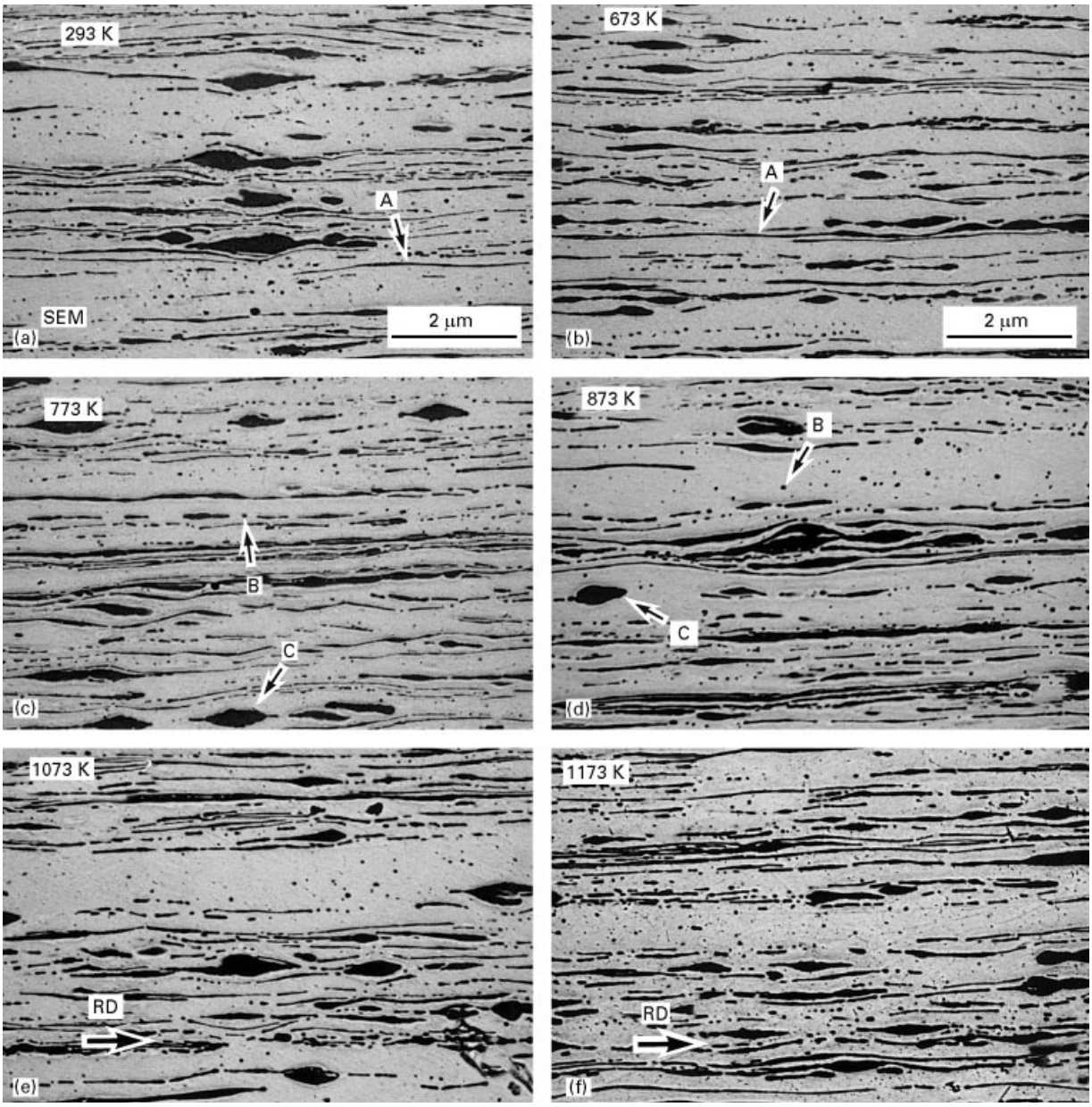

Figure 3 SEM back-scattering images of the *in-situ* composite aged at (a) room temperature, (b) 673 K for 1 h, (c) 773 K for 1 h, (d) 873 K for 1 h, (e) 1073 K for 1 h and (f) 1173 K for 1 h.

corresponding BF observation of the coffee-bean contrast (Fig. 4c). Therefore, it can be concluded that the precipitates in the peak hardened condition are the Cr GP zones which are fully coherent with the Cu matrix and have the same f.c.c. lattice parameter. The SAD patterns of the precipitates in the overaged condition have also been examined. The result confirms that these precipitates are the Cr b.c.c. phase having a KS orientation relationship, the same as that in dilute Cu–Cr alloy.

The above description of Fig. 4 is concerned with only the majority of Cr precipitates at each ageing condition. Owing to the diversification of the Cr precipitation, not every precipitate observed in each sample matches this description. For example, although most of the Cr precipitates in Fig. 4c exhibit the coffee-bean contrast, several of them are needle like and closer to the b.c.c. Cr phase in Fig. 4d. However, the SAD patterns from these precipitates cannot be detected because of their limited number and size as well as the instrument restriction. Although a large shear stress is present with the coherent b.c.c. Cr phase, it can still form and grow on the habit plane of $\{3\,3\,5\}_{Cu}$ along the invariant line of $\langle 5\,6\,1\rangle_{Cu}$ to minimize the strain energy, as is well illustrated in previous work [29, 39]. Since the Cr precipitates obtained at 773 K for 1 h are still Cr GP zones, it is almost impossible for the Cr precipitates at a lower ageing temperature of 673 K for 1 h (Fig. 4b) to have a b.c.c. Cr lattice. This point was further verified by means of HREM, with the results displayed in Section 3.5.

3.4.2. Cr ribbon

The most significant difference between Cu–Cr *in-situ* composite and dilute Cu–Cr alloy is the existence of Cr ribbon as the *in-situ* reinforcing element. Since no

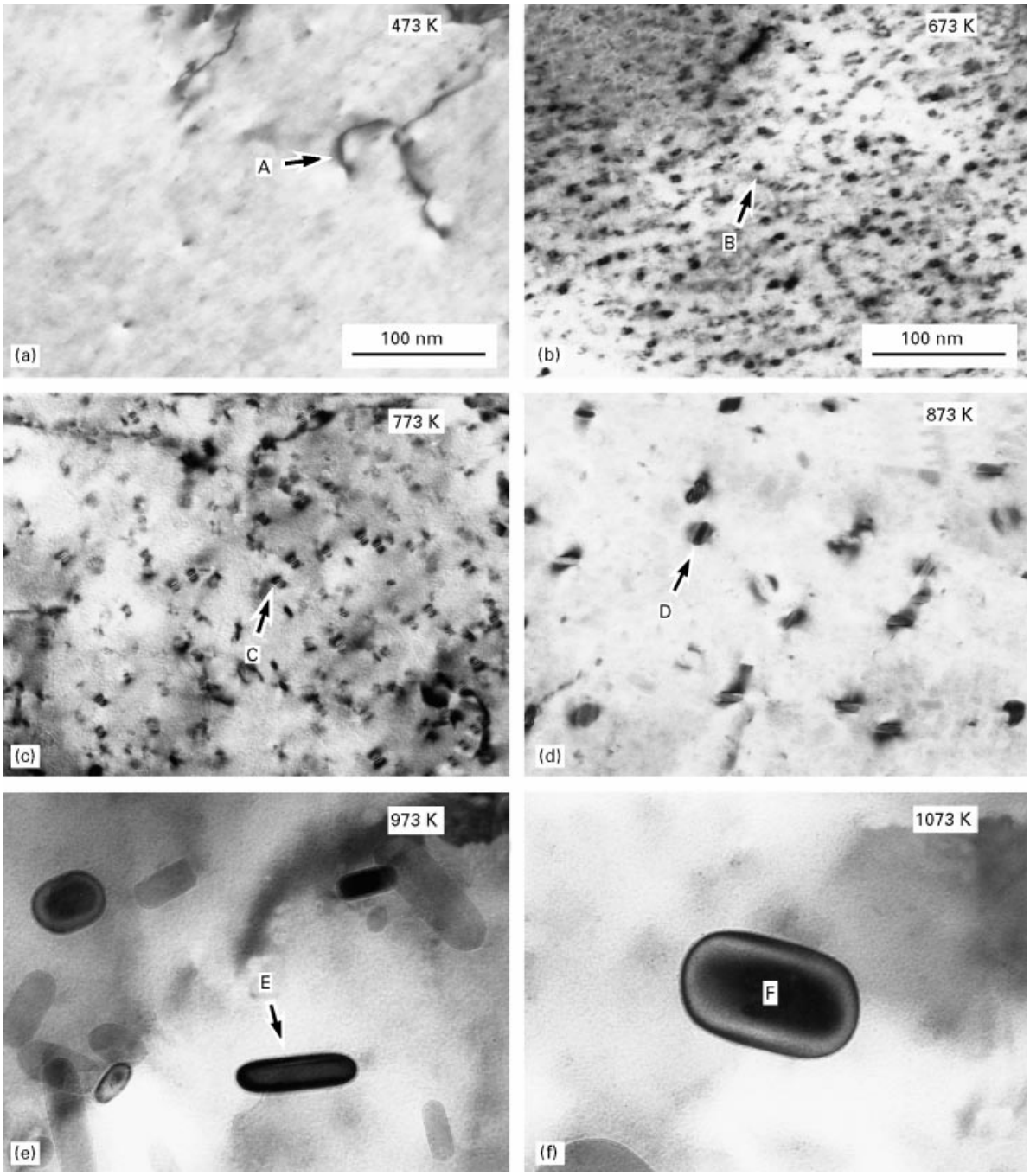

Figure 4 TEM BF images of the Cu matrix aged at (a) 473 K for 1 h, (b) 673 K for 1 h, (c) 773 K for 1 h, (d) 873 K for 1 h, (e) 973 K for 1 h and (f) 1073 K for 1 h. The orientation is close to $\langle 0\,1\,1 \rangle_{Cu}$.

TABLE I The sizes and spacings of Cr precipitates in the Cu matrix at different ageing temperatures measured from Fig. 4: NA, not applicable

Temperature (K)	Cr precipitates	Average size (nm)	Average spacing (nm)
473	None	NA	NA
673	Cr-rich cluster	9	26
773	Cr GP zone	15	42
873	Coherent Cr b.c.c. phase	20	79
973	Incoherent Cr b.c.c. phase	94	178
1073	Incoherent Cr b.c.c. phase	137	> 500

measurable hardening effect can be detected from the Cr ribbon by means of the microhardness testing, it is necessary to examine them microscopically to confirm the phenomenon. Fig. 6a is the BF image of a Cr ribbon in the water-quenched condition. A heterogeneous distribution of Cu GP zones with a coffee-bean contrast A, and the Cu equilibrium phase B were observed. This agrees with our previous report of the

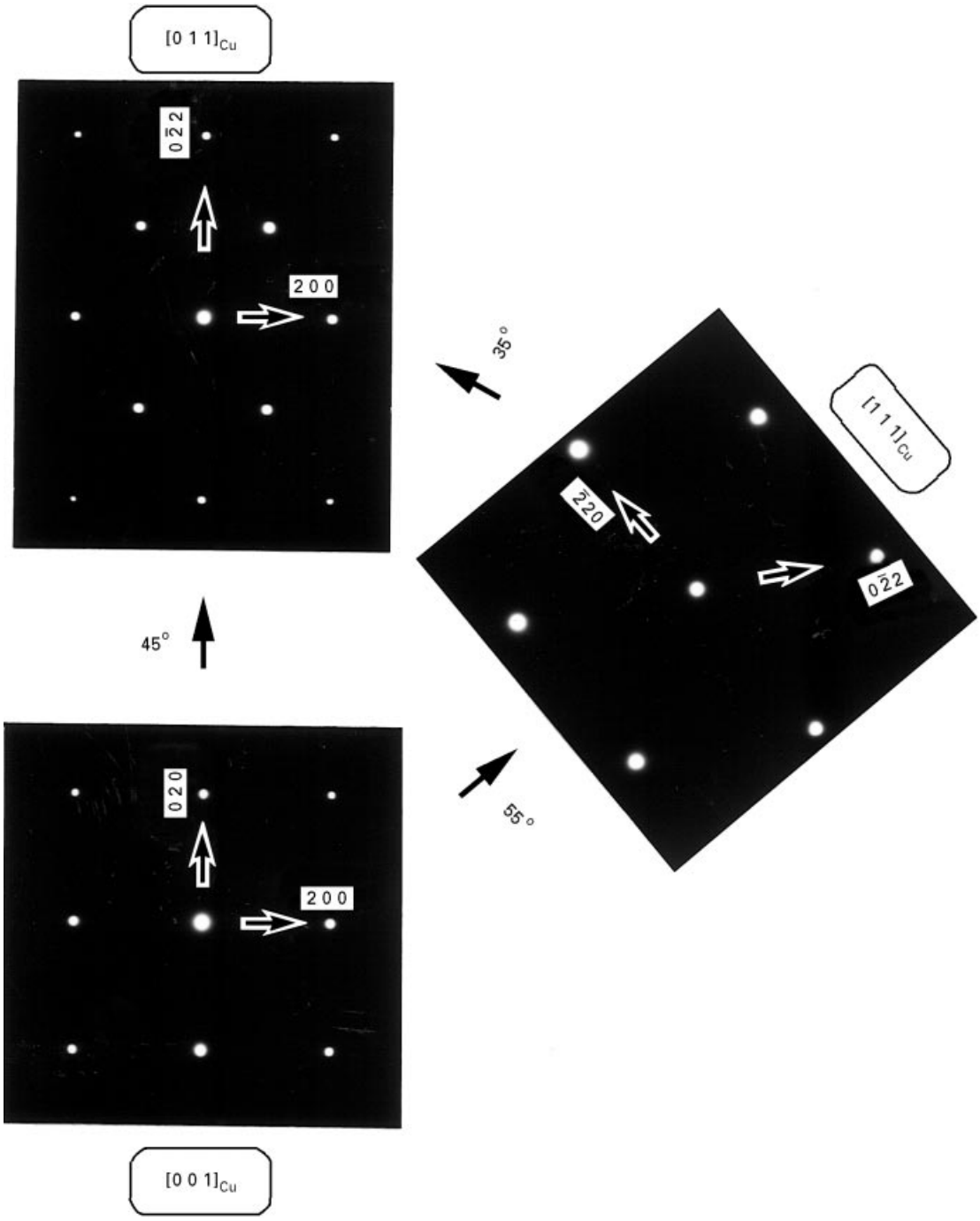

Figure 5 TEM SAD patterns of the Cu matrix in different orientations, aged at 773 K for 1 h.

existence of a nanoscale Cu-rich cluster in the heavy cold-rolling state [22]. The following heat treatment leads to evolution of these Cu-rich clusters into the Cu GP zones and the Cu equilibrium phases. Fig. 6b shows the BF image of a Cr ribbon in the peak hardened condition (773 K for 1 h). The Cu equilibrium phase was also observed. The specimens in other ageing conditions have been examined, and similar results were obtained. Since the Cu precipitates in the Cr ribbon are only of very limited number and do not display strong evolution during the ageing treatment, they produce little age-hardening effect. Therefore, it is very difficult to characterize the changes even by microhardness testing.

Fig. 7a is the BF image showing the grain-boundary dislocations GB in the Cr ribbon in the water-quenched condition. This is quite different from the observation in the heavy cold-rolling state [22]. Although heavy deformation was experienced, Cr ribbons were found mostly retaining a single-crystal structure [22]. However, the subsequent solution treatment results in the strain relaxation and recrystallization of the Cr ribbons. Fig. 7b shows the grain-boundary dislocations GB in the Cr ribbon observed in an overaged condition (1073 K for 1 h), and no significant difference can be found. The samples with the other ageing treatments have been examined, and similar results were obtained. Since the observed grain

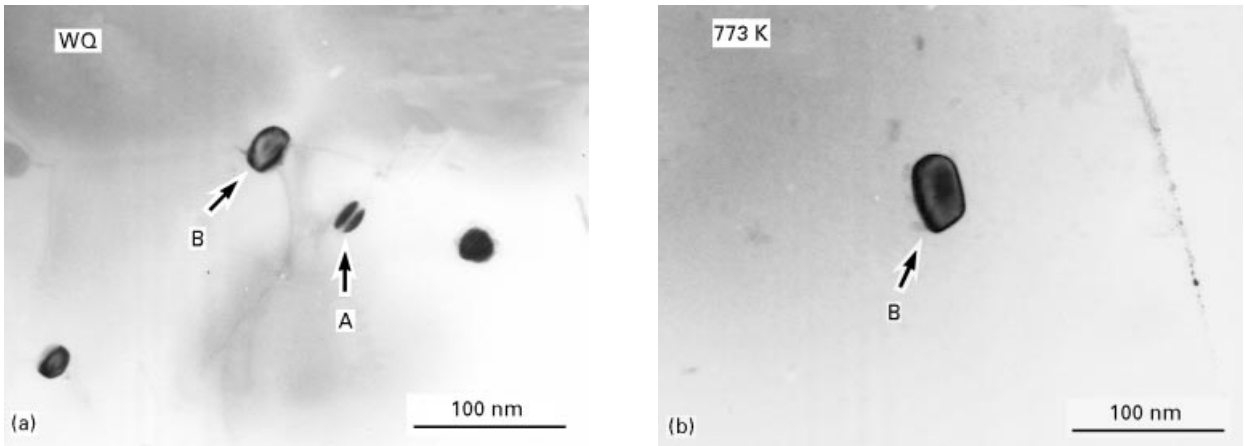

Figure 6 TEM BF image of the Cu precipitates in Cr ribbon: (a) water-quenching condition; (b) aged at 773 K for 1 h.

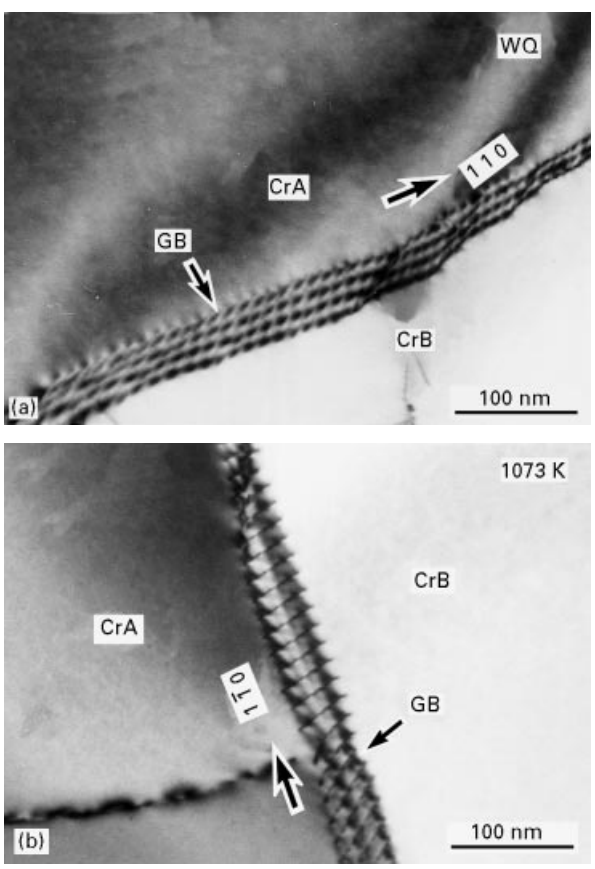

Figure 7 TEM BF image of the grain boundary in Cr ribbon: (a) water-quenching condition; (b) aged at 1073 K for 1 h.

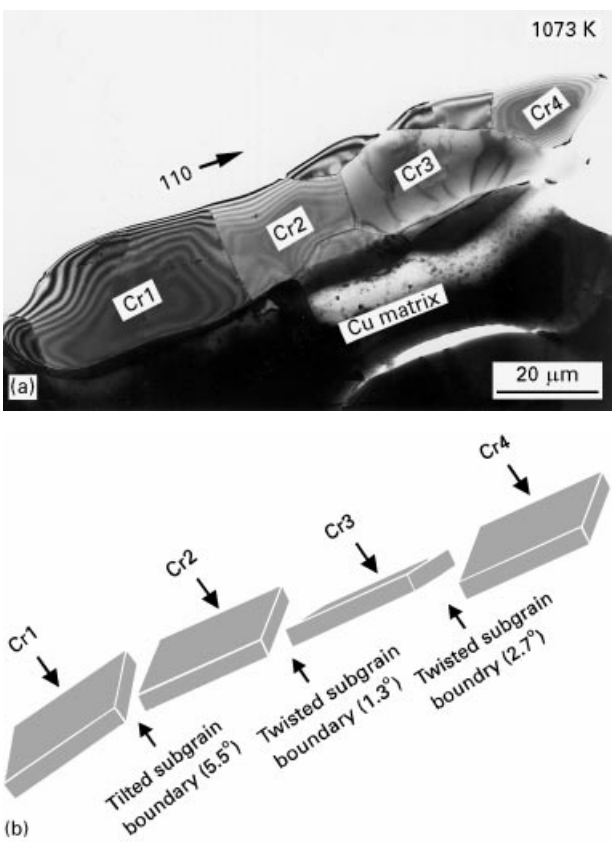

Figure 8 TEM BF image of a Cr ribbon aged at 1073 K for 1 h; (b) the corresponding illustration of grain-boundary angles measured by the large-angle CBED technique.

boundaries of Cr ribbon in various ageing conditions are composed of dislocations, they should be either tilted or twisted small-angle grain boundaries. This was verified by measuring directly the angle between two grains in the Cr ribbons with the large-angle convergent-beam electron diffraction (CBED) technique which provides the best accuracy. Fig. 8a shows the BF image of a Cr ribbon with length of around 128 μm and width of around 20 μm, aged at 1073 K for 1 h. The longitudinal direction of the Cr ribbon was determined to be $\langle 1\,1\,0 \rangle_{Cr}$, which is consistent with our previous study of the Cr deformation texture structures [23]. As schematically illustrated in Fig. 8b, the grain boundaries between four large grains Cr1 to Cr4 were all determined to be small-angle tilted or twisted grain boundaries with a maximum angle of 5.5°. The samples in the other ageing conditions have also been examined, the results are similar.

Although the instability of *in-situ* reinforcing elements has been studied recently in other Cu *in-situ* composites by Hong *et al.* [17], they reported only the phenomena of spheroidization and discontinuous coarsening due to large local gradients of stored energy in the heavily cold-worked two-phase structures. To the present authors' knowledge, this is the first experimental evidence concerning the recrystallization

of Cr *in-situ* reinforcing elements. It is suggested that, when annealing at a high temperature, the recrystallization is also an important factor accounting for the instability of *in-situ* reinforcing elements. A further investigation is now being carried out to study the effect of cold rolling on the ageing and stability of the *in-situ* composite. Because of the difficulties of sample preparation, it has been impossible to obtain sufficient information about the interface between the Cu matrix and Cr ribbons although that is very important.

3.5. High-resolution electron microscopy observation

The Cr-rich cluster in the Cu matrix has been examined by means of HREM. Fig. 9a shows the HREM image of a Cr-rich cluster in the $[0\,1\,1]_{Cu}$ orientation after ageing at 673 K for 1 h. The Cr-rich cluster, around 3 nm in size, displays a darker contrast than the surrounding Cu matrix. More information can be obtained by improving the image of the cluster with computer image-processing techniques, and the result is shown in Fig. 9b. It can be seen that the Cr-rich cluster appears to be fully coherent with the surrounding Cu matrix on the $[0\,1\,1]_{Cu}$ projection and has the same two-dimensional lattice although lattice distortion exists. Since the habit plane of the b.c.c. Cr precipitate phase is $\{3\,3\,5\}_{Cu}$ [39], it cannot display a HREM image like this along the $[0\,1\,1]_{Cu}$ orientation, no matter whether coherent or incoherent. Therefore, it is concluded that the Cr-rich cluster has the same f.c.c. lattice as that of the Cu matrix.

The existence of a Cr GP zone in the Cu matrix has also been confirmed by the same method. Fig. 10a is the HREM image of a Cr GP zone in the Cu matrix in the $[0\,1\,1]_{Cu}$ orientation after ageing at 773 K for 1 h. The Cr GP zone, around 10 nm in size, shows a similar coffee-bean strain contrast as that observed by analytical TEM (Fig. 4c) but with more detailed information. Theoretically, a typical HREM image indicates a phase contrast under the multibeam conditions while a typical BF image suggests a diffraction contrast under the two-beam conditions [45]. The strain contrast should be much weaker under the multibeam conditions. However, in the present experiment, owing to the small lattice parameter of Cu matrix as well as the limited size of the diffraction aperture, only six

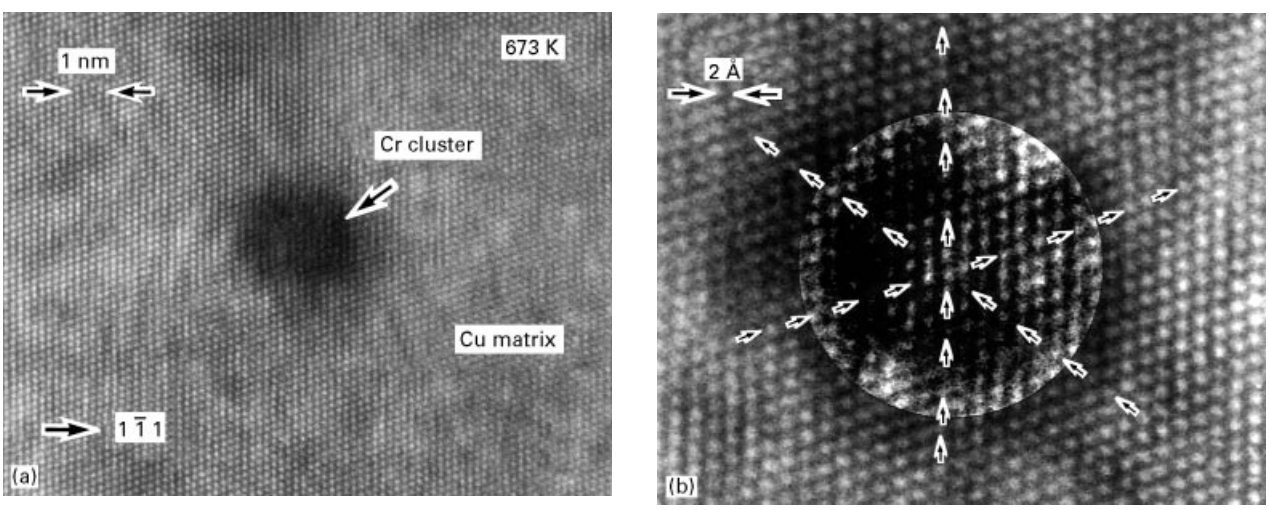

Figure 9 (a) HREM image of the Cr-rich cluster in the Cu matrix in the $[0\,1\,1]_{Cu}$ orientation aged at 673 K for 1 h; (b) computer-processed image showing the coherency of the cluster.

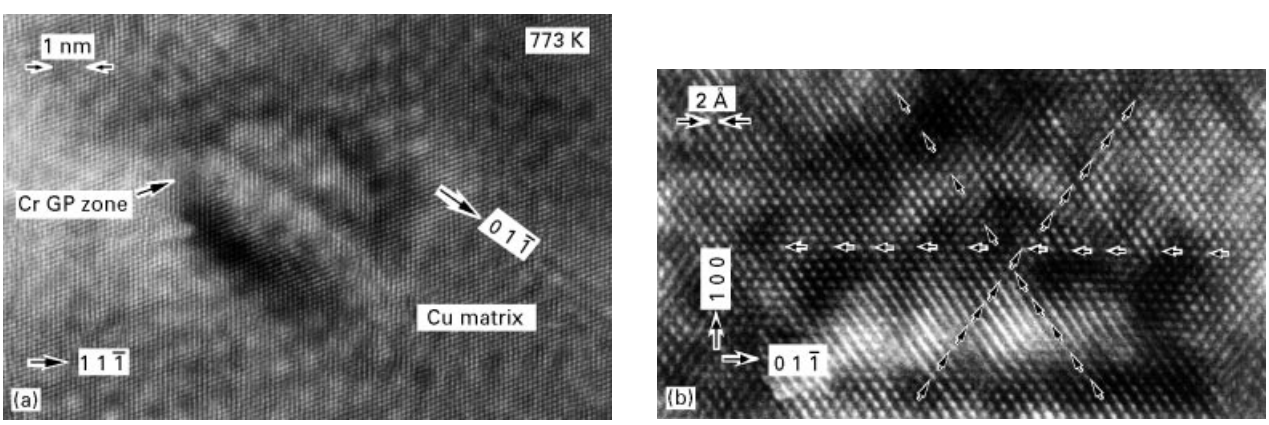

Figure 10 (a) HREM image of the Cr GP zone in the Cu matrix in the $[0\,1\,1]_{Cu}$ orientation aged at 773 K for 1 h; (b) computer-processed image showing the coherency of the GP zone.

diffraction beams (i.e., $(2\,0\,0)_{Cu}$, $(\bar{2}\,0\,0)_{Cu}$, $(1\,\bar{1}\,1)_{Cu}$, $(\bar{1}\,1\,\bar{1})_{Cu}$, $(\bar{1}\,\bar{1}\,1)_{Cu}$ and $(1\,1\,\bar{1})_{Cu}$) can be included for the HREM imaging. Therefore, the effect of diffraction contrast cannot be ignored. The HREM image of half the GP zone has also been computer processed, and the result is displayed in Fig. 10b. It can be seen that the Cr GP zone is also fully coherent with the surrounding Cu matrix on the $[0\,1\,1]_{Cu}$ projection and has the same two-dimensional lattice although there is strong lattice distortion.

4. Conclusions

1. On ageing for 1 h at different temperatures, the peak hardness occurs at around 773 K while the peak electrical conductivity occurs at around 873 K.

2. Nanoscale Cr-rich clusters were observed in the Cu matrix in the underaged condition, which matches the results of hardness testing and electrical conductivity measurement as well as the theoretical prediction.

3. The precipitates in the Cu matrix in the peak hardened condition are identified to be Cr GP zones, which are fully coherent with the Cu matrix and have the same f.c.c. lattice.

4. The Cr precipitation sequence in the Cu matrix is found to be supersaturated Cu solid solution → nanoscale Cr-rich cluster → Cr GP zone → coherent Cr b.c.c. phase → incoherent Cr b.c.c. phase.

5. Solution treatment leads to the recrystallization of Cr ribbons and the formation of small-angle grain boundaries.

6. The Cr ribbon as the reinforcing element displays no measurable ageing effect after the high-temperature solution treatment.

Acknowledgements

The authors would like to express their gratitude to the Science and Technology Agency (Japan) for the financial support. The technical support from Dr K. Ogawa, Dr Y. Tsubokawa and Mr K. Mihara is highly appreciated. Acknowledgement should also be made to Dr A. F. Whithouse (University of Leicester, UK), Dr M. Kajihara (Tokyo Institute of Technology, Japan) and Professor M. Tanino (Tohoku University, Japan) for fruitful discussions.

References

1. D. RAABE and U. HANGEN, *Acta Mater.* **44** (1996) 953.
2. F. HERINCHAUS, D. RAABE and G. GOTTSTEIN, *Acta Metall. Mater.* **43** (1995) 1467.
3. W. A. SPITZIG and B. BINER, *J. Mater. Sci.* **28** (1993) 4623.
4. J. D. VERHOEVEN, L. S. CHUMBLEY, F. C. LAABS and W. A. SPITZIG, *Acta Metall. Mater.* **39** (1991) 2825.
5. W. A. SPITZIG, J. D. VERHOEVEN, C. L. TRYBUS and L. S. CHUMBLEY, *Scripta Metall. Mater.* **24** (1990) 1171.
6. C. L. TRYBUS and W. A. SPITZIG, *Acta Metall.* **37** (1989) 1971.
7. J. D. VERHOEVEN, H. L. DOWNING, L. S. CHUMBLEY and E. D. GIBSON, *J. Appl. Phys.* **65** (1989) 1293.
8. W. A. SPITZIG, A. R. PELTON and F. C. LAABS, *Acta Metall.* **35** (1987) 2427.
9. J. D. VERHOEVEN, F. A. SCHMIDT, E. D. GIBSON and W. A. SPITZIG, *J. Metals* **38** (1986) 20.
10. J. D. VERHOEVEN, E. D. GIBSON, F. A. SCHMIDT and D. K. FINNEMORE, *J. Mater. Sci.* **15** (1980) 1449.
11. C. BISELLI and D. G. MORRIS, *Acta Metall. Mater.* **44** (1996) 493.
12. *Idem.*, *Acta Metall. Mater.* **42** (1994) 163.
13. G. A. JERMAN, I. E. ANDERSON and J. D. VERHOEVEN, *Metall. Trans. A* **24** (1993) 35.
14. W. A. SPITZIG, L. S. CHUMBLEY, J. D. VERHOEVEN, Y. S. GO and H. L. DOWNING, *J. Mater. Sci.* **27** (1992) 2005.
15. Y. S. GO and W. A. SPITZIG, *ibid.*, **26** (1991) 163.
16. J. D. VERHOEVEN, S. C. CHUEH and E. D. GIBSON, *ibid.* **24** (1989) 1748.
17. S. I. HONG, M. A. HILL, Y. SAKAI, J. T. WOOD and J. D. EMBURY, *Acta Metall. Mater.* **43** (1995) 3313.
18. Y. SAKAI, K. INOUE and H. MAEDA, *ibid.* **43** (1995) 1517.
19. Y. SAKAI, K. INOUE, T. ASANO, H. WADA and H. MAEDA, *Appl. Phys. Lett.* **59** (1991) 2965.
20. Y. SAKAI, K. INOUE, T. ASANO and H. MAEDA, *J. Jpn Inst. Metals* **55** (1991) 1382.
21. Y. JIN, K. ADACHI, T. TAKEUCHI and H. G. SUZUKI, *Appl. Phys. Lett.* **69** (1996) 1391.
22. *Idem.*, *Mater. Sci. Engng* **A212** (1996) 149.
23. Y. JIN, K. ADACHI, T. TAKEUCHI and H. G. SUZUKI, *Mater. Sci. Engng* **A212** (1996) 149.
24. K. ADACHI, Y. TSUBOKAWA, T. TAKEUCHI and H. G. SUZUKI, *Jpn Jnl. Inst. Met.* **61** (1997) 391.
25. T. TAKEUCHI, K. TOGANO, K. INOUE and H. MAEDA, *J. Less-Common Metals* **157** (1990) 25.
26. S. NISHIKAWA, K. NAGATA and S. KOBAYASHI, *J. Jpn Inst. Metals* **30** (1986) 302.
27. H. SUZUKI, M. KANNO and I. KAWAKATSU, *ibid.* **33** (1969) 628.
28. R. W. KNIGHTS and P. WILKES, *Metall. Trans.* **4** (1973) 2389.
29. G. C. WEATHERLY, P. HUMBLE and D. BORLAND, *Acta Metall. Mater.* **27** (1979) 1815.
30. T. KAMIJO and H. FUKUTOMI, *Phil. Mag. A* **48** (1983) 685.
31. *Idem.*, *ibid.* **53** (1986) 439.
32. *Idem.*, *J. Jpn Inst. Metals.* **51** (1987) 988.
33. T. KAMIJO, T. FURUKAWA and M. WATANABE, *Acta Metall. Mater.* **36** (1988) 1763.
34. W. KOSTER and W. KNORR, *Z. Metallkde* **45** (1954) 350.
35. R. O. WILLIAMS, *Trans. Amer. Soc. Metals* **52** (1960) 530.
36. Y. KOMEN and J. REZEK, *Metall. Trans. A* **6** (1975) 549.
37. J. STOBRAWA and Z. RDZAWSKI, *Scripta Metall.* **21** (1987) 1269.
38. U. DAHMEN, M. J. WITCOMB and K. H. WESTMACOTT, *ibid.* **22** (1988) 1867.
39. C. P. LUO, U. DAHMEN and K. H. WESTMACOTT, *Acta Metall. Mater.* **42** (1994) 1923.
40. P. HIRSCH, A. HOWIE, R. B. NICHOLSON, D. W. PASHLEY and M. J. WHELAN, in "Electron microscopy of thin crystals" (Robert E. Krieger Publishing, Malabar, FL, 1977) p. 327.
41. K. HONO, T. SAKURAI and I. J. POLMEAR, *Scripta Metall. Mater.* **30** (1994) 695.
42. Y. M. KOO, S. M. SHAPIRO and L. E. TANNER, *ibid.* **36** (1988) 591.
43. Y. M. KOO and J. B. COHEN, *ibid.* **37** (1989) 1295.
44. K. BINDER, *Rep. Prog. Phys.* **50** (1987) 783.
45. J. M. COWLEY, in "Diffraction physics" (Elsevier, Amsterdam, 1990) p. 203.

Received 28 October 1996
and accepted 4 August 1997